

Multi-scale modeling of hemodynamics in the cardiovascular system

Hao Liu^{1,2} · Fuyou Liang² · Jasmin Wong³ · Takashi Fujiwara¹ · Wenjing Ye³ · Ken-iti Tsubota¹ · Michiko Sugawara¹

Received: 12 December 2014 / Revised: 17 February 2015 / Accepted: 17 February 2015 / Published online: 14 August 2015
© The Chinese Society of Theoretical and Applied Mechanics; Institute of Mechanics, Chinese Academy of Sciences and Springer-Verlag Berlin Heidelberg 2015

Abstract The human cardiovascular system is a closed-loop and complex vascular network with multi-scaled heterogeneous hemodynamic phenomena. Here, we give a selective review of recent progress in macro-hemodynamic modeling, with a focus on geometrical multi-scale modeling of the vascular network, micro-hemodynamic modeling of microcirculation, as well as blood cellular, subcellular, endothelial biomechanics, and their interaction with arterial vessel mechanics. We describe in detail the methodology of hemodynamic modeling and its potential applications in cardiovascular research and clinical practice. In addition, we present major topics for future study: recent progress of patient-specific hemodynamic modeling in clinical applications, micro-hemodynamic modeling in capillaries and blood cells, and the importance and potential of the multi-scale hemodynamic modeling.

Keywords Multi-scale modeling · Macro-hemodynamics · Micro-hemodynamics · Cardiovascular system · Endothelial cell

1 Introduction

The human cardiovascular system (CVS) is the biological system responsible for transporting nutrients to tissues/organs, taking waste products away, delivering hormones, and thereby maintaining an appropriate environment for survival and the normal functioning of organs/tissues. The cardiovascular system is a closed-loop, multiple scale, complex vascular network comprised of arteries, capillaries, veins, and the heart, circulating multi-phase fluid that contains serum, blood cells, gases, heat, and various other particles.

Multi-scale modeling of hemodynamics in the cardiovascular system can be a useful tool for simulation-based predictive medicine and has potential applications in research and clinical practice. In this review, we overview recent studies on the macro-hemodynamic modeling of the arterial tree, geometrical multi-scale hemodynamic modeling of the heterogeneous composition of the vascular network, micro-hemodynamic modeling of the micro-vascular system (MVS), and the cellular mechanics of blood. Unlike other reviews in literature, for instance, the patient-specific modeling of the cardiovascular system by Taylor and Figueroa [1], pulse-wave propagation by van de Vosse and Stergiopoulos [2], fluid–structure interactions by Holzapfel and Ogden [3], geometrical multi-scale modeling by Taelman et al. [4], and flow in the microcirculation by Popel and Johnson [5], the present review aims at providing an in-depth systemic description of the framework, methodology, and strategy associated with multi-scale modeling of hemodynamics in the cardiovascular system.

In Sect. 2, macro-hemodynamic modeling in the cardiovascular system is discussed, where focus is placed on geometrical multi-scale modeling. We discuss the strategy

✉ Hao Liu
hliu@faculty.chba-u.jp

¹ Graduate School of Engineering, Chiba University, 1-33, Yayoi-cho, Inage-ku, Chiba, Japan

² Shanghai Jiao Tong University and Chiba University International Cooperative Research Center (SJTU-CU ICRC), 800 Dongchuan Road, Minhang District, Shanghai, China

³ The Hong Kong University of Science and Technology (HKUST), Kowloon, Hong Kong, China

and methodology of the geometrical multi-scale hemodynamic modeling concerning key issues associated with 0D–1D coupling and 0D/1D–3D coupling, as well as the applications of patient-specific modeling in clinical practice. In Sect. 3, we provide a description of the strategy and methodology of the micro-hemodynamic modeling by reviewing some recent studies on 1D models of the micro-vascular system, blood cell models, cellular and subcellular models, and models accounting for endothelial cell remodeling. We describe in detail a multi-scale modeling approach applied to study the interplay between micro-hemodynamics at the level of endothelial cells and macro-hemodynamics in arteries. Finally, we give a summary and discuss some future directions.

2 Modeling macro-hemodynamics in the cardiovascular system

2.1 Overview

As an anatomically complex system, the cardiovascular system is of heterogeneous composition, featuring different hemodynamic characteristics throughout its various components. The difficulty in modeling such heterogeneous hemodynamics has led to the concept of geometrical multi-scale modeling [4]. The basic idea of multi-scale modeling is to couple low-dimensional (0D, 1D) to high-dimensional (3D) models so that the resulting model can reasonably capture the hemodynamic phenomena of concern whilst demanding affordable computational resource. A typical application of multi-scale modeling method is to analyze the detailed flow field in a specific region of interest while taking into account the global hemodynamic behaviours (e.g., pulse wave propagation in the arterial tree).

2.2 Equations and parameters of physiological fluid dynamics at large vessels

2.2.1 Three-dimensional hemodynamic models with rigid / compliant walls

Blood in the CVS can be represented as an incompressible fluid with its fluid dynamic behaviour approximated by a Newtonian fluid model governed by the Navier–Stokes equations. Arterial vessels usually have compliant walls, which deform significantly due to the pulsation of blood pressure. One of the major challenges in the field of cardiovascular mechanics is to model interactions between blood flow and deforming vascular walls [1,3,4]. The interaction between blood flow and vessel walls can be resolved by coupling two sets of equations of the incompressible Navier–Stokes equations for blood flow and the elastodynamics equations governing the motion of vascular walls:

$$\begin{aligned} \rho_f \left(\frac{\partial \mathbf{u}_f}{\partial t} + \mathbf{u}_f \cdot \nabla \mathbf{u}_f \right) &= \nabla \cdot \boldsymbol{\sigma}_f + \mathbf{f}_f, \\ \nabla \cdot \mathbf{u}_f &= 0 \quad \text{in } \Omega^f, \\ \boldsymbol{\sigma}_f &= -p\mathbf{I} + \boldsymbol{\tau}, \end{aligned} \quad (1)$$

and

$$\rho_w \frac{\partial \mathbf{u}_w}{\partial t} = \nabla \cdot \boldsymbol{\sigma}_w + \mathbf{f}_w \quad \text{in } \Omega^w, \quad (2)$$

where Ω^f denotes the fluid domain, \mathbf{u}_f the flow velocity, \mathbf{f}_f the body forces acting on the blood per unit of mass, $\boldsymbol{\sigma}_f$ the Cauchy flow stress tensor including the pressure p , the unit tensor \mathbf{I} and the viscous stress tensor $\boldsymbol{\tau}$; Ω^w denotes the vessel wall domain, \mathbf{u}_w the wall velocity, \mathbf{f}_w the body forces acting on the blood vessel by external tissues and $\boldsymbol{\sigma}_w$ the Cauchy wall stress tensor.

The interaction between the blood flow and the vascular structure is enforced by imposing vessel motion and dynamic equilibrium at the fluid–structure interface, such that:

$$\begin{aligned} \mathbf{u}_f &= \mathbf{u}_w \\ \boldsymbol{\sigma}_f \cdot \mathbf{n}_f &= -\boldsymbol{\sigma}_w \cdot \mathbf{n}_w \quad \text{on } \Gamma^w, \end{aligned} \quad (3)$$

where \mathbf{n}_f and \mathbf{n}_w denote the unit normal vectors, and Γ^w the interface between the blood flow and the vessel wall.

Methods in fluid–structure interactions (FSI) One of the most well known techniques used to describe fluid–structure interaction (FSI) is the Arbitrary Lagrangian–Eulerian (ALE) formulation [1,3], which is a boundary-fitting technique capable of accurately capturing the fluid–solid interface moving due to continuous changes of the fluid grid. The Navier–Stokes equations are written in a moving reference frame that follows the motion of the vascular structure interface determined by vessel motion and dynamic equilibrium. The ALE formulations were first used by Perktold et al. [6] in cardiovascular applications and there have since then been several recent applications in cerebral aneurysm, carotid-bifurcation [7], and patient-specific abdominal aortic aneurysm models [8].

The immersed boundary method (IBM), pioneered by Peskin [9], is a non-boundary-fitting formulation in a fixed Cartesian coordinate system, which was originally developed in the context of finite-difference approximations for the fluid domain. The structure that is represented with a set of nonconforming, interconnected, elastic boundary points interacts with the fluid via the introduction of body forces applied on the fluid domain at the position of the solid points. The IBM approach was used by Vigmond et al. [10] in cardiovascular applications and developed a whole-heart electro-mechano-fluidic computational framework. Closely related to the IBM formulation, the fictitious domain method

was first developed by Glowinski et al. [11] in a finite-element context by introducing Lagrange multipliers to constrain the motion of the fluid and the solid at the interface. The method has been successfully applied to FSI simulations of the aortic valve [12].

A coupled-momentum method was developed by Figueroa et al. [13] specifically for blood flow and vessel wall interaction in arteries. With the assumptions of small deformation and thin walls this method embeds the elastodynamics equations into the variation form of the fluid dynamic equations by applying the definition of a fictitious body force that drives the motion of the vessel.

Constitutive behaviour of vessel walls The most well used arterial wall constitutive equation is based on linear elastic and isotropic assumptions, which are widely recognized as an appropriate method for wall mechanics in the physiological range of intra-arterial pressures [3]. According to the adapted Moens–Korteweg equation, the relationship between the incremental elastic modulus, $E_{inc} = d\sigma/d\varepsilon$, and the pulse wave velocity (PWV) is given by

$$PWV = \sqrt{\frac{E_{inc}h}{\rho D(1 - \sigma^2)}}, \quad (4)$$

where D denotes diameter of the artery, h the wall thickness, and ρ the vessel wall density; the Poisson coefficient of the arterial wall is usually chosen as $\sigma = 0.5$, and a constant Young's modulus E_{inc} is always set to be around 0.4 MPa.

To simulate pathological situations, the nonlinear behaviour of the artery walls can be modeled with hyperelastic models or even more complex anisotropic models that account for the fibre orientation or the mechanical property changes associated with the activation of smooth muscle [3]. However, one of the main difficulties in patient-specific modeling of physiological fluid–structure interactions remains to be the in vivo determination of tissues' constitutive properties.

To take further into account the mechanical effect of surrounding tissues, an additional constitutive function is needed to relate the stress, σ_s , on the outer arterial wall surface to the displacement \mathbf{d}_s ,

$$p_0\mathbf{n} + \sigma^s\mathbf{n} + \alpha\mathbf{d}_s = 0, \quad (5)$$

where \mathbf{n} is the outward normal vector, p_0 is the hydrostatic pressure. The coefficient $\alpha = 10^4$ (dyne/cm³), which increases where the arterial wall becomes thin, is usually given empirically in order to obtain physiological arterial wall displacements [3, 14].

3D modeling with rigid walls Three-dimensional rigid wall models, where blood flow is determined by assuming that the

vascular wall is rigid and that any wall motion does not affect the flow, are often used to obtain details of the pressure and velocity fields as well as wall shear stresses in specific arterial regions of particular physiological or pathological interest such as bifurcations, aortic arch, abdominal aorta, or cerebral aneurysms [15]. Assuming a rigid wall largely simplifies the numerical approach and reduces computational effort, but is justifiable only in the cases where the wall motion is relatively small. However, when the magnitude of arterial wall deformations is large, such as in the case of the aorta whose wall deformation magnitude can reach up to 15 % [14], it becomes essential to include the effect of wall motion.

Parameters featuring 3D hemodynamics Considering the complexity of morphology and blood flow–vascular structure interaction in the CVS, proper scaling and feature characterization of complicated mechanical phenomena by introducing some key parameters is useful to identify characteristic properties of the CVS system.

For the blood flow in the CVS, three dimensionless parameters are usually employed: Reynolds number, Strouhal number, and Womersley number. The Reynolds number (Re) represents a ratio between inertial forces and viscous forces, which is often defined by a reference length (L_{ref}) usually taken as the diameter (D) of a blood vessel and a reference velocity (U_{ref}) as the mean flow velocity (U_m) at a cross-section of the vessel, such that:

$$Re = \frac{L_{ref}U_{ref}}{v} = \frac{DU_m}{v}, \quad (6)$$

where v denotes the dynamic viscous coefficient of blood. Since flow volumetric rate Q_{ref} rather than the mean velocity is often measured in the clinical settings, given the cross-sectional area A , Re can be further reformed as,

$$Re = \frac{DQ_{ref}}{vA}. \quad (7)$$

The Strouhal number (St) describes the relative influence of axial flow versus the vessel contraction, which characterizes the pulsation behaviour and vortex dynamics of the pulsatile blood flow. The Strouhal number is defined as a function of the heart beat frequency f , the vessel diameter, and the axial flow speed,

$$St = \frac{L_{ref}f}{U_{ref}} = \frac{Df}{U_m}. \quad (8)$$

The Womersley number (α) provides a better measure of the unsteadiness associated with the pulsatile flow frequency in relation to viscous effects, which is defined as,

$$\alpha = L_{ref} \left(\frac{f}{v} \right)^{\frac{1}{2}}. \quad (9)$$

It can also be written in terms of the dimensionless Reynolds number (Re) and Strouhal number (St):

$$\alpha = (2\pi Re \cdot St)^{\frac{1}{2}}. \quad (10)$$

2.2.2 One-dimensional hemodynamic models

One-dimensional (1D) governing equations for hemodynamics in a vessel can be obtained by integrating the 3D Navier–Stokes equations (Eq. (1)) over the vessel's cross-section based on a set of assumptions. Generally adopted assumptions include an axisymmetric cross-section, a uniform pressure distribution in vascular cross-section, and a cross-sectional velocity profile dominated by the axial components [16, 17]. Under these assumptions, 1D fluid dynamic equations can be derived as [18, 19]:

$$\frac{\partial A}{\partial t} + \frac{\partial Q}{\partial z} = 0, \quad (11)$$

$$\frac{\partial Q}{\partial t} + \frac{\partial}{\partial z} \left(\alpha \frac{Q^2}{A} \right) + \frac{A}{\rho} \frac{\partial P}{\partial z} = -F_r \frac{Q}{A}, \quad (12)$$

where t denotes the time and z the axial coordinate; A , Q , and P denote the cross-sectional area, volume flux, and pressure, respectively; α is the momentum-flux correction coefficient and F_r the friction force per unit length, both of which are dependent on the assumptions made for the velocity profile. For simple purpose, many studies assumed a Poiseuille or uniform velocity profile [16–19]. With a Poiseuille velocity profile, α , F_r can be derived theoretically, being $4/3$, $8\pi\nu$ (ν denotes the kinematic viscosity), respectively. More sophisticated assumptions include those taking into account the effects of vascular size [20, 21] or time-dependent changes in velocity profile during a cardiac cycle [22, 23]. It should be noted that any assumed velocity profile needs the introduction of certain simplifications and, therefore, cannot completely account for all the cross-sectional flow information, which is distributed three-dimensionally in nature. Fortunately, 1D models are usually applied to describe wave propagation phenomena in large arteries where the effects of conductive and viscous terms on wave propagation are secondary compared to arterial wall mechanics.

There are three unknowns (Q , A , and P) in Eqs. (11) and (12). In order to close the equation system, an additional equation is needed. The equation is usually obtained by formulating a tube law that relates P to A . Under in vivo conditions, the P – A relation is highly nonlinear due to the heterogeneous composition of the vessel wall (consisting of endothelium, elastin, smooth muscles, and collagen fibres with different mechanical properties), making its mathematical expression highly complex. When 1D models are applied to arteries, blood pressure usually varies in a narrow range

(e.g., between 60 and 150 mmHg), under which condition the deformation of arterial wall is small (variation in diameter is generally within 5%), and blood pressure can be related almost linearly to arterial radius. This permits a relatively simple P – A relation to be adopted [16–19, 24]:

$$P - P_e = \frac{Eh}{r_0(1 - \sigma^2)} \left(\sqrt{\frac{A}{A_0}} - 1 \right) + P_0, \quad (13)$$

where P_e is the external pressure, P_0 the reference pressure, E the Young's modulus, h the wall thickness, r_0 the radius of artery at reference pressure, and σ the Poisson's ratio. In the case where the vascular wall suffers from large deformation, such as for veins or arteries subject to external pressures that vary over a large range, Eq. (13) should be replaced by a staged function or nonlinear expression to account for the inherent nonlinearity of the P – A relation [25, 26].

To apply the 1D equations to describe fluid dynamics in a vessel network (such as the arterial tree), additional equations obtained by imposing continuity of mass flux and pressure at bifurcations are required to link the vessels [16–25]. Because of the hyperbolic characteristics of Eqs. (11–13), many numerical algorithms can be applied to solve the equation system with good convergence properties. The most frequently adopted methods are finite difference methods and finite element methods [16–25]. With respect to temporal discretization, explicit methods can avoid the management of equation matrices and simplify the treatment of boundary conditions, thus significantly reducing the difficulty of programming. However, the magnitude of the numerical time step is restricted by the Courant–Friedrichs–Lewy (CFL) condition. For problems where excessively stiff vessels are included or wall stiffness differs significantly among vessels, implicit methods would be more ideal [27].

2.2.3 Zero-dimensional (lumped parameter) models

Zero-dimensional (0D, or lumped parameter) hemodynamic models have been developed based on the Windkessel theory [28, 29]. The hypothesis underlying the theory is that the pressure in a deformable fluid container is homogeneous in space. In arteries, the spatial variation of blood pressure is small because the pressure wavelength (5–15 m) is much larger than the anatomical dimension (usually less than 1 m in length) of arteries [18], which justifies the application of the Windkessel theory to the modeling of the arterial system. The original Windkessel model employed to represent the arterial system is the so-called two-element model consisting of a compliance element and a resistance element [28]. The compliance element represents the deformable capability of large arteries, while the resistance element accounts for the viscous friction of small peripheral vessels to blood flow.

The two-element model was modified later to describe more reasonably the dynamic properties of cardiac afterload by, for example, placing a characteristic impedance element before the compliance element to reproduce the spectrum of aortic input impedance in high frequency domains [30], or introducing an inertance element to improve the comparison between simulated and measured aortic pressure waveforms [31]. Although the 0D modeling concept has originated from the Windkessel theory, mathematically, the governing equations of 0D models can be deduced from the 1D hemodynamic equations. By assuming a uniform cross-sectional area (A) distribution in the axial direction, integrating Eq. (11) over the length of a vessel gives

$$\frac{dV}{dt} = Q_{z_l} - Q_{z_0}. \quad (14)$$

Here, V represents the volume of fluid contained in the vessel; Q_{z_0} and Q_{z_l} denote the flow rate at the inlet and outlet of the vessel, respectively.

Further neglecting the conductive term in Eq. (12) and assuming a constant flow rate (Q) distribution in the axial direction, integrating Eq. (12) over the length gives

$$\frac{dQ}{dt} = \frac{P_{z_0} - P_{z_l} - RQ}{L}, \quad (15)$$

where P_{z_0} and P_{z_l} denote the hydrostatic pressures at the inlet and outlet of the vessel, respectively; R is the viscous resistance expressed as $8\pi\rho\nu(Z_l - Z_0)/A^2$ (where ρ is the density of blood); and L is the inertance of blood in the vessel, given by $\rho(Z_l - Z_0)/A$.

Further assuming a constant compliance independent of pressure for the vessel, Eq. (14) can be rewritten as

$$\frac{dP}{dt} = \frac{Q_{z_l} - Q_{z_0}}{C}, \quad (16)$$

where C is the compliance of the vessel, which can be derived from Eq. (13) via a series of mathematical managements

$$C = \frac{dV}{dP} = \frac{2r_0(Z_l - Z_0)\sqrt{AA_0}(1 - \sigma^2)}{Eh}. \quad (17)$$

As a consequence, there are three parameters (i.e., R , L , and C) and two state variables (i.e., Q and P) in the 0D equations. When several vessels are connected to form a network, Q_{z_0} and Q_{z_l} in Eq. (16) denote the inlet or outlet flow rates of the adjacent vessels.

Although Eqs. (14) and (15) are derived from fluid dynamic equations for a single vessel, they can be used to describe blood flow through many vessels. In practice, when 0D modeling methods are applied to the cardiovascular system, the system is often first divided into a set of compartments according to its anatomical configuration, with each

compartment corresponding to a certain vascular portion, such as the arterial portion, the microvascular portion and the venous portion, and so on [32,33]. Each vascular compartment can then be represented by a combination of R , L , and C to account for its hemodynamic effects. Connecting all the compartments yields a network of parameters and state variables governed by an ordinary differential equation system that can be solved using general numerical methods, such as the Runge–Kutta methods [32].

2.3 Strategy and methodology of geometrical multi-scale hemodynamic modeling

A common procedure of geometrical multi-scale hemodynamic modeling in the CVS consists of three steps: (1) decomposition of the global domain into subdomains, (2) modeling of the subdomains in different geometrical details, and (3) coupling of different models by imposing continuity of hemodynamic quantities at the interfaces between models.

2.3.1 Boundary conditions at model interfaces

Boundary conditions at the interfaces between models of different scales (0D–1D–3D) are usually formulated to guarantee the continuity of mass and pressure and the conservation of mass and momentum across the interface.

One boundary condition addresses the *flow rate problem*, namely assigning a flow rate Q_i through each of the boundaries Γ_i ($i = 1, \dots, n$), for instance, of a 3D domain, such that:

$$\int_{\Gamma_i} \mathbf{u} \cdot \mathbf{n} \, ds = Q_i. \quad (18)$$

Note that the flow rate conditions $\sum_{i=1}^n Q_i = 0$ for the 3D model must be satisfied at each time step for the rigid CFD case, whereas for FSI simulations, the difference between inflow and outflow is adjusted in the deforming fluid domain. Therefore, the flow rate boundary condition at the interfaces between 0D/1D and 3D models is implemented by imposing the 0D/1D-based flow rate to Eq. (18).

On the other hand, at the inlet and outlet, the 3D models usually require the prescription of three velocity components at each point of the discretized boundaries. However, 0D or 1D models provide only spatially averaged flow rates at each cross-section. A common approach amongst various techniques consists of prescribing an a priori selected velocity profile in terms of a flat, parabolic, or Womersley manner fitting the given flow rate, which has the drawback that the chosen velocity profile strongly affects the numerical solution in the 3D domain [4]. One well-used and relatively

effective technique is to extend the computational domain at the outlets artificially, which is usually taken as sufficiently long to have the velocities developed so as to reduce the sensitivity of the numerical solution in the zone of interest to the selected velocity profile.

The other boundary condition is the mean pressure problem in which a spatially averaged pressure P_i at each cross section of the vessel is enforced at the interface of a 3D domain, such that:

$$\frac{1}{\Gamma_i} \int_{\Gamma_i} p ds = p_i. \quad (19)$$

To ensure the continuity of the pressure at the interfaces of different scales, the averaged pressures P_i of Eq. (19) at the interfaces are assigned with the 0D/1D-based pressures at the cross-section [4].

2.3.2 0D–1D multi-scale hemodynamic models

Traditional 1D models focused solely on the arterial tree while representing the remainder of the cardiovascular system with simplified boundary conditions [33]. Frequently adopted boundary conditions consist of a flow waveform imposed at the inlet of the aorta and a set of lumped parameters connected to the distal ends of the arterial tree to account for the hydrodynamic loads of distal vasculatures [16,22,24,34]. Alternatively, a tree-structured model has been proposed to represent the hydrodynamic loads of distal vasculatures with improved spectral characteristics [35]. Such a model configuration permits a reasonable description of wave propagation/reflection in the arterial system, but may be confronted with considerable limitations under certain conditions due to its inherent insufficiency in accounting for cardiac-arterial coupling [18]. For instance, the contour of flow waveform at the aortic inlet is determined by hemodynamic interaction between the heart and the arterial system, rather than being fixed [18]. For this reason, imposing a normal flow waveform at the aortic inlet may lead to considerable deviations of simulated pressure waveforms from in vivo phenomena in the presence of severe arterial stenotic disease or cardiac dysfunction. To overcome the limitations, the concept of multi-scale modeling has been proposed. The work was pioneered by Formiagga et al. [17] who coupled a lumped parameter model of the left ventricle to a 1D model of the arterial tree. The modeling method was later developed by Liang et al. [18,19] to construct a closed-loop multi-scale cardiovascular model by coupling a 1D model of the arterial tree to a lumped-parameter model of the remaining cardiovascular system. Recently, such models have been further expanded to include a 1D model of the venous system as well [25].

2.3.3 0D/1D–3D multi-scale hemodynamic models

One strategy is to handle geometrical multi-scale models of different scales in an iterative way based on an explicit approach scheme [4]. In the explicit coupling case, the 3D-based spatially averaged flow rates derived from the boundaries of the 3D model are imposed as boundary conditions to the 0D/1D models (referred to as defective boundary conditions), which in turn compute the mean (total) pressures at the boundaries and transfer the pressure data onto the 3D model in the next time step. The 3D model with mean (total) pressures boundary conditions can then be solved following the do-nothing approach, which addresses the mean pressure and flow rate problem using variational formulations, implicitly completing the defective data set with homogeneous Neumann conditions [36]. Note that the hemodynamic quantities exchanged between the 3D and 0D/1D models can be reversed, because here only one iteration per time step is performed, the continuity of total stress and mass flow rate is not strictly preserved [37].

An approach has been proposed to overcome this defect, by introducing the Dirichlet-to-Neumann (Gauss–Seidel) iterations [7]. At each time step, an iterative coupling algorithm is introduced between the 3D and 1D solvers to reduce the pressure residuals at the interfaces to a level lower than a prescribed tolerance. This requires continuous fine-tuning of the relaxation parameter, which usually cannot guarantee convergence of the algorithm, especially when an elevated number of coupling interfaces are involved. For this problem, more robust strong coupling techniques have been developed and can be found in studies by Levia et al [38,39].

The techniques for coupling 3D models with lumped parameter (0D) models have also been developed in a similar way. An example is the coupled multi-domain method, which was developed based on the Dirichlet-to-Neumann and variational multi-scale methods [40]. The method employs a disjoint decomposition of the spatial domain into an upstream “numerical” domain and a downstream “analytical” domain, with the two domains linked by the interfaces C_{in} and C_{out} [1,41].

2.4 Patient-specific modeling and clinical applications

In this section, we present the applications of 0D–1D and 0D/1D–3D coupled models in patient-specific modeling to show the potential of geometrical multi-scale modeling and discuss the key issues from the viewpoint of clinical applications.

Coupled 0D–1D models are featured by low computational cost while having the ability to simulate both arterial wave propagation phenomena and systemic hemodynamic behaviours. Liang et al [18,19] developed a closed-loop 0D–1D multi-scale model of the human cardiovascular system

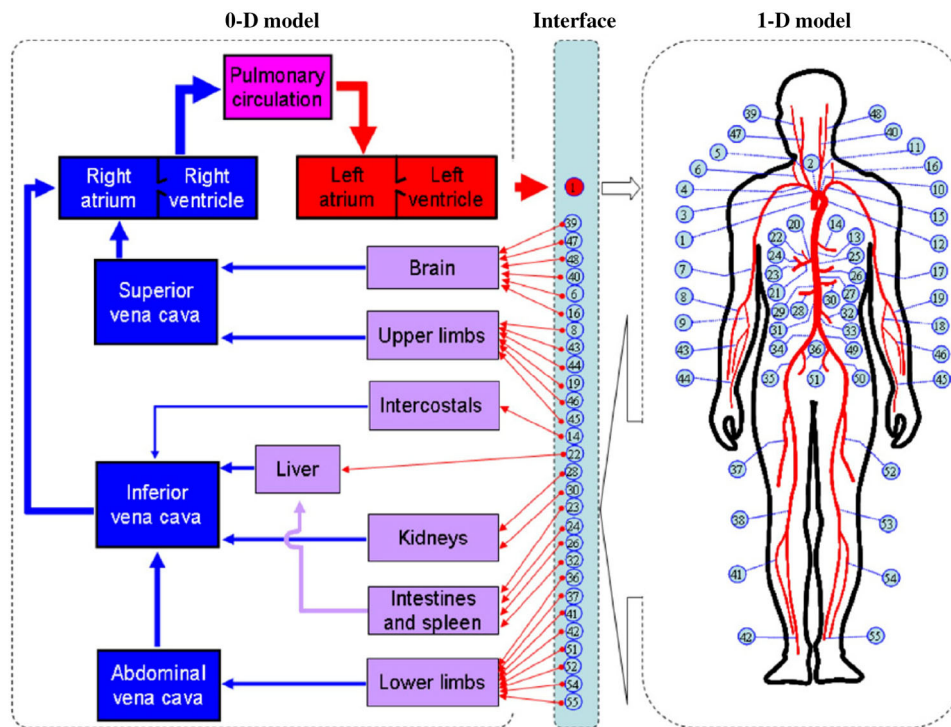


Fig. 1 Schematic description of 0D–1D modeling of the human cardiovascular system. The arterial tree consisting of the 55 largest arteries is described by a 1D model (*right*), while the remainder, including the heart, the peripheral circulation and the pulmonary circulation, is represented by a 0D model (*left*). The lumped parameter element network of a vascular system corresponding to a peripheral artery: the network consists of several serially arranged compartments including the arteriolar, capillary, venular, and venous compartments [18,19]

and studied the changes in ventricular–arterial (VA) hemodynamic coupling during aging. The model was constructed by describing the arterial tree using a 1D model coupled with a 0D model of the remainder (Fig. 1).

Figure 1 illustrates the 1D arterial tree model consisting of 55 largest arteries [18,19]. The 0D model describes the peripheral circulation, the pulmonary circulation and the heart. The vascular subsystem corresponding to each peripheral artery is described by a lumped parameter network; the “time-varying elastance” method is adopted to describe the dynamics of the four cardiac chambers. Their study found that the VA coupling index (effective arterial elastance (E_a)/left ventricular (LV) end-systolic elastance (E_{es})) at rest was well maintained during normal aging. Aging effects on arterial transmission performance is illustrated in Fig. 2, showing that aorta–periphery pulse pressure amplification diminishes gradually, and the pressure waves increasingly resemble each other during aging.

Coupled 0D–1D–3D modeling is aimed mainly at simulating local hemodynamic phenomena whilst accounting for the interactions between local and systemic hemodynamics. The study by Hsia [42] reported the application of a 0D–3D multi-scale model to predict the differences in hemodynamic impact between hybrid and surgical Norwood palliations for

hypoplastic left heart syndrome. In the study, a 3D computational fluid dynamics model of either the Norwood or the hybrid procedure was coupled to a lumped parameter description of the entire circulation. Figure 3 depicts the multi-scale models of the hybrid, Blalock–Taussig shunt (BTS), and right ventricle–pulmonary artery shunt (RVS) palliations. The 0D and 3D model were coupled by exchanging flow rate and pressure information via the interfaces. The multi-scale model predicts flow dynamics in Blalock–Taussig shunt and pulmonary arteries, as well as global hemodynamic variables including cardiac output, venous oxygen saturation, and cerebral oxygen delivery. The simulated results demonstrated that the hybrid palliation had higher pulmonary-to-systemic flow ratio and lower cardiac output.

The presence of forward flow throughout a cardiac cycle in the BTS model has been reported previously, whereas backward flow in the RVS during diastole was first found and confirmed clinically in the study (Fig. 4). In the case of hybrid palliation, diastolic runoff into the branch pulmonary arteries can occur through the ductal stent as predicted by the hybrid model. On the other hand, the simulation results also demonstrated that 33 % of forward flow in the brachiocephalic artery was reversed backward during diastole.

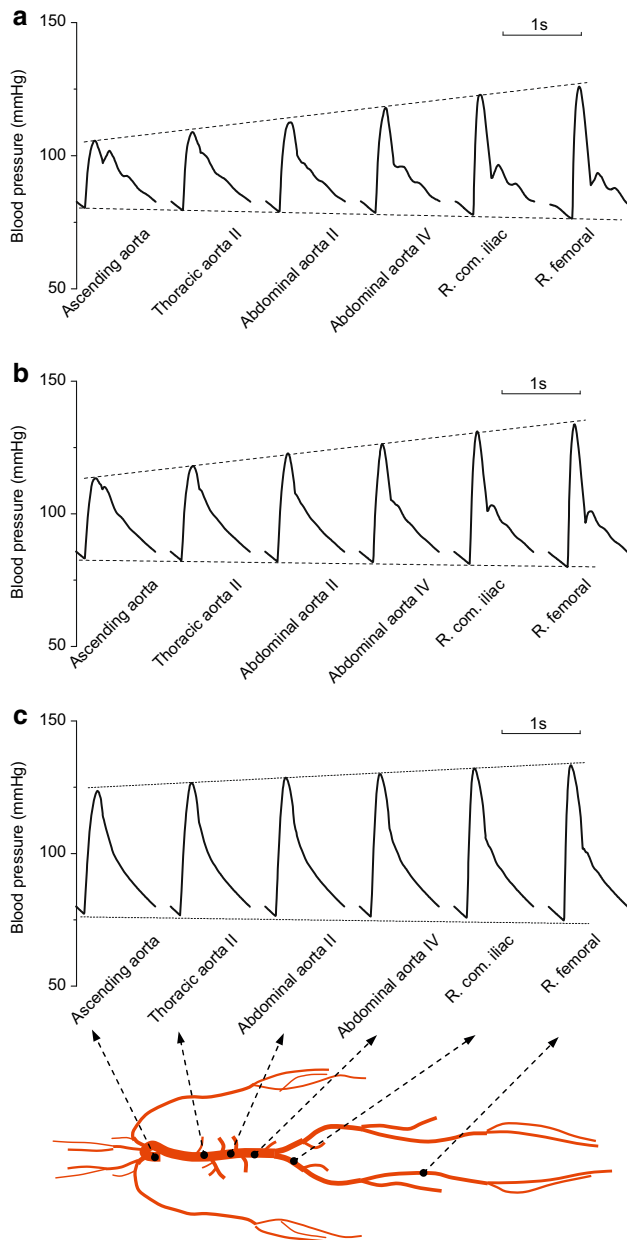


Fig. 2 Snapshots of pressure wave variation along the arterial tree at the ages of **a** 25 years, **b** 55 years, and **c** 85 years. Aorta–periphery pulse pressure amplification rate decreases with age, and, at the same time, the central and peripheral pressure waves progressively resemble each other during aging [18]

3 Modeling micro-hemodynamic in the micro-vascular system

3.1 Overview

The micro-hemodynamics in the micro-vascular system (MVS) covers a widely heterogeneous complex network of the capillaries connecting the arteriovenous system, from the cardiovascular system as a whole down to blood cells and

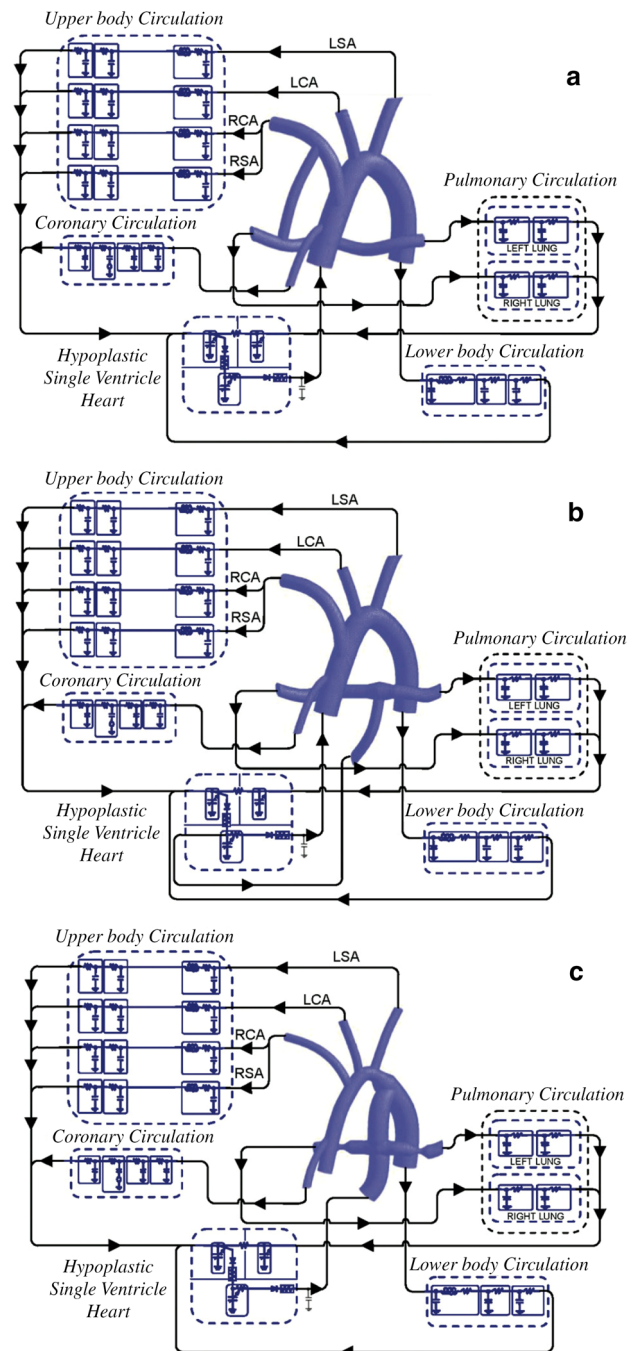


Fig. 3 Multi-scale models of **a** the modified Blalock–Taussig shunt, **b** the right ventricle–pulmonary artery shunt, and **c** the hybrid Norwood. *LSA* indicates the subclavian artery, *RSA* right subclavian artery, *LCA* left carotid artery, and *RCA* right carotid artery [42]

single cells of the vessel. Modeling studies in MVS have been done mostly at different scales with the one-dimensional (1D) micro-circulatory models on non-pulsatile and pulsatile flows, the behaviour of shape and deformation of single RBC, as well as the mechanical interaction between single RBC and plasma, and RBC to RBC interaction via plasma fluid, and

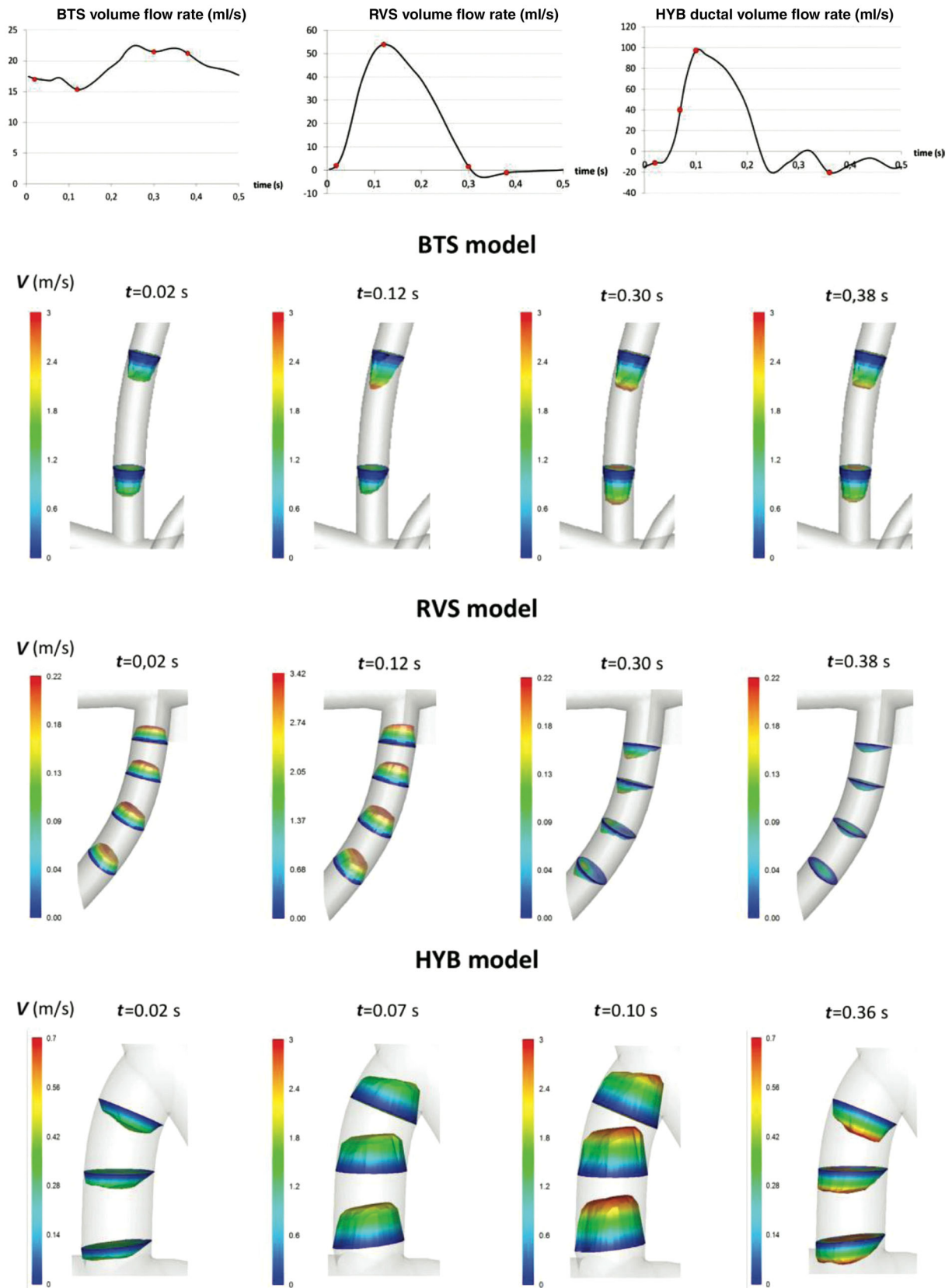


Fig. 4 Velocity profiles on various cross sections of the shunts and the ductus arteriosus in the modified Blalock–Taussig shunt (BTS; *top*), right ventricle-to-pulmonary artery shunt (RVS; *middle*), and hybrid (HYB; *bottom*) models at four time points in the cardiac cycle [42]

sub-cellular models associated with events like deformation, migration and division. On the other hand, there are still no models established for dynamic morphology and distribution (referred to as EC remodeling) of the endothelial cells (EC) on vessel walls with consideration of the multi-scale interaction between the micro-hemodynamics at EC scale and the macro-hemodynamics at vessel scale in terms of multi-scale coupling.

3.2 Strategy and methodology of micro-hemodynamic modeling

3.2.1 One-dimensional model for the MVS

Blood flow in microcirculation is pulsatile in terms of pressure and pulse wave velocity (PWV) [43], in which pulsatility has wide-ranging physiological consequences [44–46], and non-pulsatile flow is observed to be related to dysfunctions of micro-vascular systems [47–49].

Compared with steady models of microcirculation that are based on steady state concepts [50–52], dynamic models [53,54] may be capable of exploring pulse wave propagation in microcirculation. The 1D model allows the assessment of dynamic features of interest with a relatively low computational burden. One simple model for pulsatile flow in microcirculation is the Womersley method [55], but it neglects nonlinear convective terms in the momentum conservation relationship. Among the several recently developed 1D models that account for nonlinear components for complex microcirculatory networks [56], Pan et al. [27] proposed a 1D wave propagation model of microcirculation. The model was tested using the vascular network of rat mesentery as recorded by intravital microscopy experiments, which provided morphological, topological, and hemodynamic parameters [57–60]. It can be considered a generic microvasculature with respect to the heterogeneity of the network architecture and hemodynamic parameters, and thus fit for comparison between simulated results and physiological findings [61].

Governing equations were the 1D hemodynamic model in each vessel segment as well as at diverging and converging bifurcations based on the conservation of mass and momentum as shown in Eqs. (11) and (12). A pressure-area relationship of the elastic vessel similar to Eq. (13) was further introduced to close the equation set, in which the mechanical properties of the vessel wall in arterioles were considered to be similar to that of arteries [62]. The structure of capillaries and venules were assumed to be “tubes-in-gel” and were mechanically supported by external elastic components [63].

The rheological effects in microcirculation were accounted for using the Fahraeus–Lindqvist effect and the phase separation effect [64]. These effects adjust blood viscos-

ity and, consequently, flow resistance, which is relevant for hemodynamic simulations. A flow rate time-series was used as the input boundary, whereas lumped resistant boundaries [65] were coupled with the outlet nodes at the outlets.

This model is able to reproduce the dynamic characteristics of a microvascular network, including the pressure pulsatility (quantified by a pulsatility index: PI_P) and pulse wave velocity (PWV). From the main input arteriole to the main output venule, the pulsatility index obtained along arterioles declined with decreasing diameters by 66.7%. PWV, with mean values of 77.16, 25.31, and 8.30 cm/s for diameters of 26.84, 17.46, and 13.33 μ m, respectively. As shown in Fig. 5, pulsation was strongly damped in terms of PI_P from the arteriolar tree until the post capillary level and remains almost constant at a low level in the venules, indicating that damping in the arterioles prevents pressure pulsatility transmission to more distal parts of the vascular bed.

3.2.2 Blood cell models

Red blood cells (RBCs) occupy the largest volume (45%) of blood, and are thus major mechanical elements. Blood may be assumed to be a continuum fluid in large arteries and veins at which the vessel size is much larger than blood cells. In microcirculation with the RBCs compatible in size to a vessel, the blood rheology may be dominated by the RBC's morphology and deformation, the RBC–plasma mechanical interaction, and the RBC–RBC interaction via plasma fluid. All these mechanical factors may feature equally in the micro-hemodynamics of the blood as a suspension in the MVS. Therefore, significant effort has been made to develop mathematical and computational modeling of the blood cell mechanics and the micro-hemodynamics.

Single RBC mechanics RBCs that consist of an outer viscoelastic cell membrane and an inner viscous fluid usually show significant deformation properties. As such, continuum mechanics have been used to investigate the viscoelastic mechanics of the RBC membrane and viscous fluid mechanics of the inner and suspending fluids. In general, the RBC mechanics are characterized by three mechanical properties: (1) the equilibrium shape in normal and swollen cells, (2) the elongation deformation by micropipette aspiration and optical tweezers, and (3) the tumbling (T) and tank-treading (TT) motions under viscous shear flow. To understand how these three different characteristics integrally feature each other and RBC mechanics, it is essential to develop a unified and versatile computational model, which, however, has not been achieved despite extensive computational studies in the past decades [66–69].

Elastic membrane mechanics and constitutive equations A single RBC has been modeled as a fluid drop encapsulated by

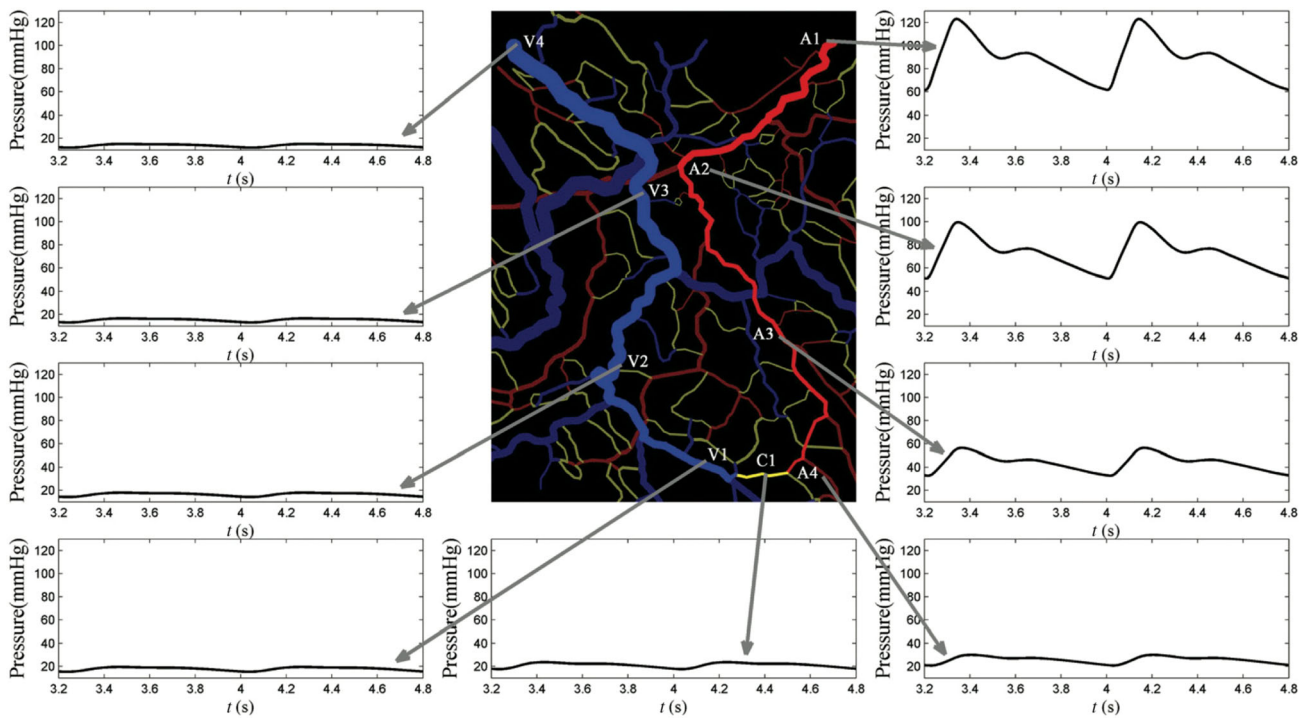


Fig. 5 The pressure waveforms of the selected segments on the arteriovenous pathway “A”. The waveforms are substantially damped from the main feeding arteriole to the capillary level and remain almost unchanged in the venular section [27]

a surface membrane. Elastic mechanics of the surface membrane are broadly divided into in-plane deformations and out-of-plane bending deformations. For constitutive equations, the in-plane shear and area dilatation elasticity may be modeled on the basis of Skalak law [70] such as:

$$T_1 = G \frac{\lambda_1}{\lambda_2} \left[(\lambda_1^2 - 1) + C_a \lambda_2^2 (\lambda_1^2 \lambda_2^2 - 1) \right], \tag{20}$$

where T_1 denotes the principal tension, λ_1 and λ_2 ($\lambda_1 \geq \lambda_2$) the principal stretches, G the shear modulus, and C_a the elastic constant that determines the modulus of local area dilatation $G(1 + 2C_a)$. The second principal tension T_2 ($T_1 \geq T_2$) is calculated by interchanging the indices 1 and 2. The out-of-plane elasticity may be modeled with the Helfrich isotropic bending energy [71] such that:

$$W_B = \frac{1}{2} B \int_A (2H - C_0)^2 dA, \tag{21}$$

where $H = \frac{1}{2}(C_1 + C_2)$ represents the spontaneous mean curvature determined by the two principal curvatures C_1 and C_2 ($C_1 \geq C_2$), C_0 the natural state curvature, and B the bending rigidity. In addition, the elastic energy associated with a change in the global membrane area A from its reference A_0 may be introduced with the area dilatation modulus k_A as

$$\Gamma_A = \frac{k_A}{2} \left(\frac{A - A_0}{A_0} \right)^2 A_0. \tag{22}$$

Note that if the modulus k_A is significantly larger than the elastic constants G , $C_a G$, and B , Γ_A can operate as a penalty function for the constraint conditions $A = A_0$.

Single RBC mechanics by natural state Based on observations of relatively large deformations of RBCs in response to external forces, the constitutive Eqs. (20) and (21) of the cell membrane have been identified with a set of viscoelastic constants. On the other hand, a natural state of the cell membrane, which is defined as the zero-stress configuration of the membrane, is another major factor that determines the elastic deformation. A cell membrane’s natural state has not yet been made clear, and two representative natural states for the elastic deformation have been assumed: the biconcave disk, which is the shape of a normal RBC (i.e., discocyte), and the sphere, which is the shape of a reticulocyte (precursor of a mature RBC). Recently, Tsubota and Wada [67–69] have proposed the intermediate shapes ($0 < \alpha < 1$) between a sphere ($\alpha = 0$) and a biconcave disk ($\alpha = 1$) to model the membrane’s natural state with respect to the in-plane shear deformation (Fig. 6a). Here, the parameter α was introduced as a measure of non-uniformity of the natural state, and the intermediate shapes were described on the basis of the linear interpolation of the geometries as

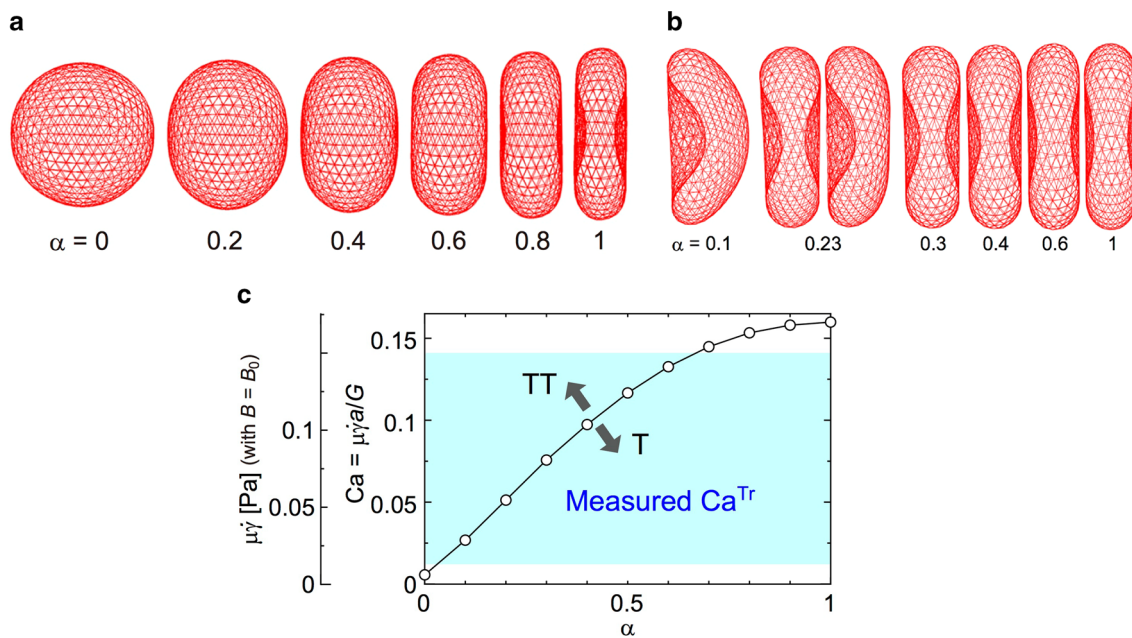


Fig. 6 **a** An RBC model of the membrane’s natural state with respect to in-plane shear deformation, **b** *biconcave discoid shape* of a normal RBC or a *cupped shape* of a diseased state at an equilibrium state in a stationary fluid, and **c** an experimentally measured critical shear stress with transition between TT and T motions under viscous shear flow [69]

$$\mathbf{x}_{0_i} = \mathbf{x}'_{0_i} \sqrt{A_0/A'_0}, \mathbf{x}'_{0_i} = \mathbf{x}_{Sphere_i} + \alpha (\mathbf{x}_{BD_i} - \mathbf{x}_{Sphere_i}), \tag{23}$$

where \mathbf{x}_{0_i} , \mathbf{x}_{Sphere_i} , and \mathbf{x}_{BD_i} are the positions of the material point i on the natural state of the cell membrane, a sphere, and a BD shape, respectively, and A' represents the surface area of the BD shape determined by \mathbf{x}'_{0_i} . The natural state, represented by C_0 , for the out-of-plane bending deformation in Eq. (21) is assumed constant over the membrane, by considering an in-plane fluidic nature of the lipid bilayer in the membrane.

The intermediate shapes for the natural state plays a key role in determining whether a single RBC takes a biconcave discoid shape of a natural state or a cupped shape of a diseased state at an equilibrium state in a stationary fluid (Fig. 6b) [71]. The membrane’s natural state is also important to reproduce an experimentally measured critical shear stress at which transition between TT and T motions under viscous shear flow occurs [70,71] (Fig. 6c) because the natural state controls elastic energy barrier against TT motions [1]. Their results suggested α values as 0.2–0.3, and suggest that detailed modeling of cell membrane’s natural state is one of a key to establish a unified model for RBC mechanics. We note that in simulating the equilibrium shape mechanics, the membrane’s bending rigidity at the transition of equilibrium shapes from the biconcave disk to the cup is different by an order of magnitude, depending upon a type of bending model employed, which points to the importance of the choice of bending models [72].

Furthermore, it is noted that such single RBC mechanics substantially influences the mechanical interactions between multiple RBCs in terms of blood rheology as a function of hematocrit [69]. The cell–cell interaction plays an important role in the blood rheology as well as in platelet aggregation, i.e., the thrombus, another major topic associated with computational modeling of cell biomechanics [73–75]. In the boundary element method (BEM) to couple membrane deformation and fluid flow, the velocity \mathbf{u} at the nodal point \mathbf{r}_i on the RBC membrane Λ is calculated by the integral equation:

$$\mathbf{u}(\mathbf{r}_i) = \frac{2}{1+\lambda} \left| \mathbf{u}^\infty(\mathbf{r}_i) - \frac{1}{8\pi\mu} \int_A \Delta \mathbf{f}(\mathbf{x}) \cdot \mathbf{G}(\mathbf{x}, \mathbf{r}_i) d\Lambda(\mathbf{x}) + \frac{1-\lambda}{8\pi} \int_A^{PV} \mathbf{u}(\mathbf{x}) \cdot \mathbf{T}(\mathbf{x}, \mathbf{r}_i) \cdot \mathbf{n}(\mathbf{x}) d\Lambda(\mathbf{x}) \right|, \tag{24}$$

where \mathbf{u}^∞ denotes the undisturbed velocity, $\Delta \mathbf{f}$ is the hydrodynamic traction jump across the membrane, \mathbf{n} is the unit vector normal to the membrane pointing into the suspending fluid, \mathbf{G} and \mathbf{T} are the Green’s functions of Stokes flow for the velocity and stress, respectively, and PV is the principal value. Because the traction jump $\Delta \mathbf{f}$ is balanced by the elastic load on the membrane in the absence of membrane inertia, and $\Delta \mathbf{f}$ on the element e may be calculated from the element nodal force by adopting a linear shape function [71]. While application of the BEM to RBCs motion in a channel flow has been achieved, numerical challenges still

remain with respect to the balance between accuracy and computer time. Recently the immersed boundary method (IBM) based on Eulerian coordinate system has been proposed and demonstrates high potential as a practical tool to model both single cell motion and blood rheology owing to multiple cell motions. In addition, the particle methods based on the Lagrangian coordinate system are also useful to simulate motions of deformable RBCs in capillary vessels [73, 74, 76], in which the particles can directly track the solid-fluid interface while showing good numerical stability rather than that of the IBM in modeling large deformations of blood cells. This method has also been applied to simulate the formation and destruction of thrombi due to their interaction with platelets, interactions among monocytes, platelets and a vascular surface, and the adhesive dynamics of rolling cells.

3.2.3 Cellular and subcellular models

Compared with blood cell models, models for single cellular events such as deformation, migration, and division are still limited. One reason may be the difficulty to handle a multi-physical problem. Not only mechanical events, but chemical reactions and sometimes even electrical signalling are important factors for single cell events. In addition, the multi-scale problems in both time and size further enhance the difficulty in numerical modeling of single cellular events. Here, we focus on one of the cellular events, “cell migration”, while considering the related molecular events inside the cell [77–80].

Cell migration is a highly integrated system that characterizes many cellular events of multi-cellular organisms. In general, cell migration involves several interdependent components: the formation of cell polarity, protrusion at the leading edge, its adhesion to the extracellular matrix (ECM), detachment of the membrane from the ECM at the cell rear, and translocation of the cell body forward. The actin cytoskeleton and focal adhesions play a central role in those processes [81].

There are several actin structures relating to cell protrusion during migration. *Lamellipodia*, the primary site of actin polymerization, are surface-attached sheet-like membrane protrusions at the cell’s leading edge consisting of a network of branched actin filaments including several actin-binding proteins [82–84]. *Filopodia* are thin finger-like protrusions from the leading edge, containing parallel bundles of short actin filaments [85, 86].

As for the actin structures relating to whole cell migration, we know that actin stress fibres make up a critical structure during cell migration. They are cross-linked by a periodic distribution of α -actinin [87], with myosin often involved in some instances [88], which results in their contractibility. Three types of stress fibres have been distinguished: ventral stress fibres, dorsal stress fibres, and transverse arcs. Ventral

stress fibres, anchored at each end by focal adhesions, mainly exist at the cell rear and are involved in the translocation of the cell body forward. Dorsal stress fibres are typically associated at just one end of the nearest focal adhesions or inside the lamella at the cell front, and they elongate toward the dorsal section of the cell and terminate at transverse arcs that join the stress fibres parallel to the leading edge of the cell [89]. Recently, signalling and molecular pathway for assembly of three types of stress fibres has been well studied [90, 91].

Although various actin structures have been studied and their functions relating to the migration system is partially understood, the whole system has not yet been clarified. The next step will be the systematic understanding of the role of various types of stress fibres during cell migration. Therefore, both mathematical and computational modeling and experimental observation would be of great importance to provide powerful tools to explore novel mechanisms at cellular scale.

Since actin filaments are one of the relatively rigid cytoskeletal structures of the cell, they could be modeled as simple elastic rods. On the other hand, actin filaments are not passive structures, but active self-organizing materials that dynamically and autonomously change their length via chemical signals. In addition, actin structures inside lamellipodia, filopodia, and stress fibres are composed of complex network of actin filaments and several actin-binding proteins. Therefore, how to handle such a multi-physics problem seems to be a key in developing useful and effective computational models based on the cellular mechanics and dynamics.

3.2.4 Endothelial cells remodeling and multi-scale hemodynamic modeling

Endothelial cells (ECs) are constantly changing in response to their environment. Both in vitro and in vivo experiments show that ECs have different cell morphologies when exposed to various mechanical forces [92]. There has been evidence supporting the influence of hemodynamics on vascular remodeling [93], and many EC biological responses have been shown to be shear-sensitive including those regulating cell morphology [94–96]. The ECs forming a single cell layer lining the lumen in the intima layer of arteries are significantly involved in the pathogenesis of atherosclerosis, a common but dangerous affliction of the arterial wall [97].

The effect of the hemodynamics of blood flow on the arterial wall and the endothelial cells that line them have been studied for many years by measuring biological markers in response to changing flow patterns [98]. However, the influence of the EC morphology and distributions, in particular under disturbed flow conditions, still remains an open question. We propose to modify current CFD techniques in order to generate a more accurate model that includes the influence of EC morphology distribution as well as its dynamics

on flow patterns (shear stresses, etc.) to gain further knowledge on how mechanical stresses from blood flow affect ECs remodeling dynamics and vice versa.

EC remodeling: a dynamic process of morphology and distribution under disturbed flow conditions ECs are capable of modifying their overall shape by regulating the organization of internal cytoskeletal components, which is a dynamic remodeling process, in order to achieve a shape that maintains a pre-existing tension equilibrium within the cell. The tension created by the cytoskeleton must balance out against the external forces imposed on the cell surface [99]. Tensegrity is determined through continuous tension, local compression, and the dependence of shape stability on a pre-stress [100].

ECs also regulate many other pathways including those of permeability, inflammation, cell adhesion, vessel dilation, and cell proliferation in response to mechanical stress. This may be due to the altered cell programs from the rearrangement of cell components from the morphological change. Therefore, ECs play an important regulatory role in many cardiovascular diseases. In physiological conditions, arteries remodel outwards resulting in the overall dilation of the vessel when exposed to high shear stress. This is a homeostatic measure to ensure that the overall shear stress value of remains near a constant value of 1–6 dyne/cm² in the arteries and 10–70 dyne/cm² in the veins [92].

The pathways for cytoskeletal remodeling and those necessary for activation of the biomarkers of many cardio-

vascular diseases are interlinked. Many of the gene changes and biomolecular markers caused by shear stress have been experimentally confirmed to occur in atherosclerosis (Fig. 7) [101], aneurysms, and other cardiovascular pathologies. Disturbed flow has long been associated with these pathologies, such as the irregular flow in artery bends and bifurcations where atherosclerosis preferentially occurs, as well as the disturbances caused by venous valves resulting in varicose veins and venous insufficiency. Experimental data has shown that the pathways mentioned above are activated by shear stress and are responsible for the physiopathology of cardiovascular pathologies [92].

Multi-scale coupling between micro-hemodynamics at EC level and macro-hemodynamics at vessel level: an unsolved, open problem in the CVS Despite the great importance of CFD towards our understanding of hemodynamics and its relation to cardiovascular pathologies, the construction of computational models uses assumptions and simplifications, such as the no-slip boundary, that could lead to skewed data. The accuracy of the plaque geometry has a great deal of influence on the results [102]. A choice of boundary conditions can greatly affect the quantification of hemodynamic forces on the vessel wall [103]. In order to achieve more accurate results, a more accurate model would have to be used.

It is hypothesized that the rounder, more pronounced shape of the ECs at atherosclerosis prone locations has a significant effect on flow patterns that has not been accounted for in current computational fluid models. Atomic force

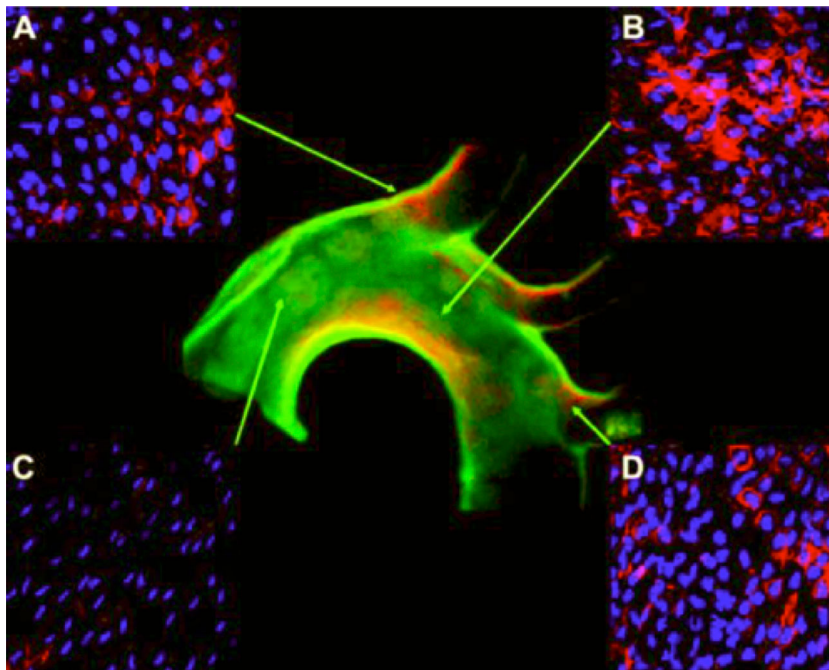


Fig. 7 Immunohistochemical stain for VCAM-1 in a mouse aortic arch reveals greater expression at the inner curvature where flow is disturbed [92]

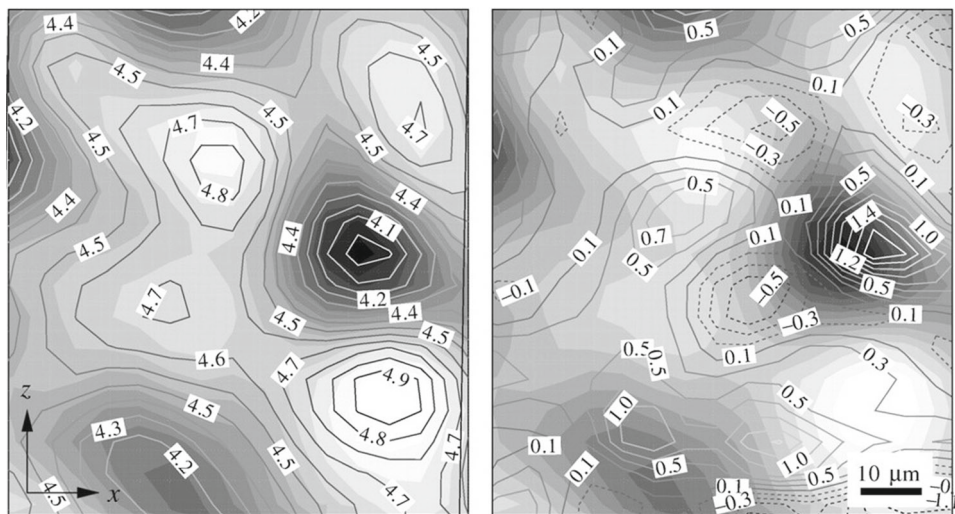


Fig. 8 Contours of shear stress (*left*) and contours of constant wall pressure (*right*) over cell surface colour contours. Brighter colour indicates greater surface height [105]

microscopy has been used to show that sheared cells aligned with the flow have a significantly reduced height (measured from base junctions to peak height above the nucleus) and that shear gradient in the direction of the flow was reduced by 50%. The study also showed that the bovine ECs used were smooth and round when not experiencing any flow stimulus, while the ones under a flow environment had small protrusions 50–100 nm in height. Control cells had a height difference of $(3.39 \pm 0.79) \mu\text{m}$, height to length ratio of 0.11 ± 0.025 , and aspect ratio of 1.12 ± 0.31 . Sheared cells, on the other hand, had a height difference of $(1.77 \pm 0.52) \mu\text{m}$, a height to length ratio of 0.045 ± 0.009 , and an aspect ratio of 2.16 ± 0.53 . These values were used to calculate maximum shear stress and maximum shear stress gradient (18 and 18140 dyne/cm^2 for control; 14 and 8220 dyne/cm^2 for sheared) using an analytical solution technique by Satcher et al. [104] for a laminar flow with shear of 10 dyne/cm^2 .

Microscopic particle image velocimetry was used to analyze shear stress and pressure at $25 \mu\text{m}$ from the wall on individual ECs in a flow chamber showed that their distribution is different over the cell surface due to the geometry of the cell itself. The vector field of laminar, steady flow on ECs forming a surface with a maximum height difference of $3.7 \mu\text{m}$ over a fluorescent image of the cells showed that flow over nucleic bulges or other high points was slower than over low points of the cells. Computed cell topography of contours of constant pressure and shear stress (calculated from Navier–Stokes and the velocity profiles) were overlaid on colour contours of cell height (Fig. 8). It was found that maximum values differed by 2.1 dyne/cm^2 for pressure stresses and 1.3 dyne/cm^2 for shear stresses. Pressure acts downward at the leading edge of the cell and upward at the trailing edge

[105] resulting in an asymmetrical wedge shaped cell with leading edge slope being smaller than trailing edge slope [106]; this can be useful in counteracting the shear-induced moment, since the more elongated the EC, the greater the moment due to pressure. These results demonstrate that both shear and pressure forces analyzed at a subcellular level affect the local net force felt at different locations on the cell as well as the global resultant force on the entire cell. They are, therefore, necessary for understanding how mechanical forces influence vascular diseases [105].

This can be further corroborated with a study that developed a mathematical model to analyze the forces on a cell nucleus approximated as a semi-ellipsoid and adjusted parameters to minimize force. For a fixed cell length, total force decreased as cell height decreased; while for a fixed cell height, total force decreased as the cell hump was elongated in the direction of the flow. Optimizing both cell height and cell length in the direction of the flow to find a minimum, they found it to correspond well with a width of $6.6 \mu\text{m}$, length of $14.8 \mu\text{m}$, and height of $1.77 \mu\text{m}$ as found by other in situ studies. This shows that in vivo dimensions for the ECs come close to a theoretical force minimum. This decrease in force can be attributed to a decrease in traction. However, not all ECs take the same shape, which suggests the influence of other forces than shear [107].

Keeping in mind that a cell is a deformable entity and not fixed in shape, numerical analyses have been critical for determining the correct non-uniform distribution of shear stresses experienced by the cell. It is suggested that this activates receptors correspondingly, which could reflect the non-homogenous nature of EC regulation [108]. These studies on cellular-level hemodynamics reveal that ECs are subjected to different forces depending on their shape.

As current models do not account for ECs, it is a goal to integrate the effect of EC morphology on fluid flow at a micro-scale as boundary condition information in simulations near the arterial wall. However, it would be impractical to run large-scale simulations with EC geometry on entire arteries. In order to simplify the addition of EC information to CFD modeling, it would be a feasible way to implement a new boundary condition derived from micro-scale simulations of an EC covered surface, instead of using a no-slip boundary condition, for macro-scale vessel CFD simulations.

This technique is hopefully able to reveal new information about the hemodynamic forces present in the cardiovascular system in physiological and pathological conditions, and by providing a more realistic flow map, allow for further investigation in the link between mechanical forces and endothelial dysfunction in atherosclerosis. This multi-scale CFD technique would confirm the importance of ECs on flow conditions as well as provide insight on why and what is achieved when ECs align in laminar flow, and how this relates to cardiovascular pathologies. This knowledge could be useful in clinical applications for diagnosis and prognosis of cardiovascular diseases, as well as provide suggestions for treatment methods. When this multi-scale modeling is available, we will be able to deal with the following problems: (1) how ECs significantly affect macro-hemodynamics; (2) why ECs align in a stress-dependent way during laminar flow and whether it minimizes friction-based drag; (3) whether ECs can achieve a shear stress minimized morphology & distribution in disturbed flow; (4) how EC morphology & distribution influence disturbed macro-scale hemodynamics under pathological conditions; and (5) whether disturbed flow at bifurcations disrupts EC remodeling and how that relates to various cardiovascular pathologies.

4 Conclusion

Multi-scale modeling of hemodynamics in the CVS is believed to be a useful and powerful tool in cardiovascular research and clinical practice. The multi-scale hemodynamic modeling may be clarified in two ways: at the macro-scale handling the geometrical multi-scale hemodynamic modeling of the vascular network, and at the micro-scale with the modeling of the microcirculation, the blood cell mechanics and the interactions between endothelial cells and arterial vessel mechanics.

With respect to the macro-hemodynamic modeling, the 0D models are convenient and very versatile for studying flow rates and pressures of either the arterial circulation or the specific organs, and for defining the peripheral boundary conditions for 1D and 3D models; the 1D models of the arterial circulation are effective and highly suitable for studying wave-propagation phenomena in the arterial tree as well

as interactions between local (3D model-based) and global (1D model-based) hemodynamics; and the 3D models as an image-based model of the region of the interest are essential and the only way to provide local flow information of velocity vectors and wall shear stresses with/without consideration of compliant vessel wall mechanics. Among the 0D, 1D, and 3D models, the 1D models have the greatest potential and are believed to be major topics as a future task in both cardiovascular research and clinical practice. The 1D models are able to be applied to the closed loop models of the complete cardiovascular system, accounting for both the pulmonary and systemic circulation including the venous system and the heart [18, 19]. Furthermore, when performing patient-specific simulation under different physiological and pathological conditions, some autonomic nervous system and auto-regulation models should be established and coupled with the closed loop cardiovascular system model so as to ensure the homeostatic mechanisms, which allows studying, for instance, the impact of baroreflex dysfunction on the local and global hemodynamics.

In the micro-hemodynamic modeling, the 1D models again show great potential in predicting the microcirculation of capillaries whereas blood cell models with consideration of membrane structures and interactions between internal and external liquids are still major topics. The endothelial cell remodeling under different shear stress situations and the interplay between such micro-cardiovascular mechanics at cellular scale and the macro-hemodynamics at vessel scale, however, are still open questions. This remodeling leads to changes in compliance and probably shear-based resistance, affecting shear stress distributions at sites with pathological diseases (stenosis and aneurysms, etc.), and may even influence wave propagation and reflection characteristics of the arterial tree. This is another multi-scale model to integrate our knowledge of the micro-biomechanics in EC and the macro-hemodynamics in the CVS, and may be a major topic for future study.

Acknowledgments Hao Liu was partly supported by Grant-in-Aid for Scientific Research (Grant (B)17300141), JSPS and by Research and Development of the Next Generation Integrated Simulation of Living Matter, JST, a part of the Development and Use of the Next Generation Supercomputer Project of the MEXT, Japan. Fuyou Liang was supported by the National Natural Science Foundation of China (Grant 81370438) and the SJTU Medical Engineering Cross-cutting Research Foundation (Grant YG2012MS24). Ken-iti Tsubota was partly funded by a Grant-in-Aid for Challenging Exploratory Research (Grant 25630046), JSPS. He also thanks RIKEN for supporting the computing facilities essential for the completion of this study. Financial support provided by HKUST to JW is acknowledged.

References

1. Taylor, C.A., Figueroa, C.A.: Patient-specific modeling of cardiovascular mechanics. *Annu. Rev. Biomed. Eng.* **11**, 109–134 (2009)

2. van de Vosse, F., Stergiopoulos, N.: Pulse wave propagation in the arterial tree. *Annu. Rev. Fluid Mech.* **43**, 467–499 (2011)
3. Holzapfel, G.A., Ogden, R.W.: Constitutive modelling of arteries. *Proc. R. Soc. Lond. A* **466**, 1551–1597 (2010)
4. Taelman, L., Degroote, J., Verdonck, P., et al.: Modeling hemodynamics in vascular networks using a geometrical multiscale approach: numerical aspects. *Ann. Biomed. Eng.* **41**, 1445–1458 (2013)
5. Popel, A.S., Johnson, P.C.: Microcirculation and hemorheology. *Annu. Rev. Fluid Mech.* **37**, 43–69 (2005)
6. Perktold, K., Rappitsch, G.: Mathematical modeling of arterial blood flow and correlation to atherosclerosis. *Technol. Health Care* **3**, 139–151 (1995)
7. Formaggia, L., Gerbeau, J.F., Nobile, F., et al.: On the coupling of 3D and 1D Navier–Stokes equations for flow problems in compliant vessels. *Comput. Methods Appl. Mech. Eng.* **191**, 561–582 (2001)
8. Wolters, B.J.B.M., Rutten, M.C.M., Schurink, G.W.H., et al.: A patient-specific computational model of fluid–structure interaction in abdominal aortic aneurysms. *Med. Eng. Phys.* **27**, 871–883 (2005)
9. Peskin, C.S.: The immersed boundary method. *Acta Numer.* **11**, 479–517 (2002)
10. Vigmond, E.J., Hughes, M., Plank, G., et al.: Computational tools for modeling electrical activity in cardiac tissue. *J. Electrocardiol.* **36**, 69–74 (2003)
11. Glowinski, R., Pan, T.W., Hesla, T.I., et al.: A fictitious domain approach to the direct numerical simulation of incompressible viscous flow past moving rigid bodies: application to particulate flow. *J. Comput. Phys.* **169**, 363–426 (2001)
12. Hart, J.D., Peters, G.W.M., Schreurs, P.J.G., et al.: A three-dimensional computational analysis of fluid–structure interaction in the aortic valve. *J. Biomech.* **36**, 103–112 (2003)
13. Figueroa, C.A., Vignon-Clementel, I.E., Jansen, K.E., et al.: A coupled momentum method for modeling blood flow in three-dimensional deformable arteries. *Comput. Methods Appl. Mech. Eng.* **194**, 5685–5706 (2006)
14. Reymond, P., Crosetto, P., Deparis, S., et al.: Physiological simulation of blood flow in the aorta: comparison of hemodynamic indices as predicted by 3-D FSI, 3-D rigid wall and 1-D models. *Med. Eng. Phys.* **35**, 784–791 (2013)
15. Sugimoto, K., Takahara, Y., Mogi, K., et al.: Blood flow dynamic improvement with aneurysm repair detected by a patient-specific model of multiple aortic aneurysms. *Heart Vessels* **29**, 404–412 (2014)
16. Sherwin, S.J., Formaggia, L., Peiro, J., et al.: Computational modelling of 1D blood flow with variable mechanical properties and its application to the simulation of wave propagation in the human arterial system. *Int. J. Numer. Methods Fluids* **43**, 673–700 (2003)
17. Formaggia, L., Lamponi, D., Tuveri, M., et al.: Numerical modeling of 1D arterial networks coupled with a lumped parameters description of the heart. *Comput. Methods Biomech. Biomed. Eng.* **9**, 273–288 (2006)
18. Liang, F.Y., Takagi, S., Himeno, R., et al.: Biomechanical characterization of ventricular–arterial coupling during aging: a multi-scale model study. *J. Biomech.* **42**, 692–704 (2009)
19. Liang, F.Y., Takagi, S., Himeno, R., et al.: Multi-scale modeling of the human cardiovascular system with applications to aortic valvular and arterial stenosis. *Med. Biol. Eng. Comput.* **47**, 743–755 (2009)
20. Devault, K., Gremaud, P.A., Novak, V., et al.: Blood flow in the circle of Willis: modeling and calibration. *Multiscale Model. Simul.* **7**, 888–909 (2008)
21. Bessems, D., Rutten, M., van de Vosse, F.: A wave propagation model of blood flow in large vessels using an approximate velocity profile function. *J. Fluid Mech.* **580**, 145–168 (2007)
22. Reymond, P., Merenda, F., Perren, F., et al.: Validation of a one-dimensional model of the systemic arterial tree. *Am. J. Physiol.* **297**, 208–222 (2009)
23. Huo, Y., Kassab, G.S.: A hybrid one-dimensional/Womersley model of pulsatile blood flow in the entire coronary arterial tree. *Am. J. Physiol. Heart Circ. Physiol.* **292**, H2623–H2633 (2007)
24. Alastruey, J., Parker, K.H., Peiro, J., et al.: Modelling the circle of Willis to assess the effects of anatomical variations and occlusions on cerebral flows. *J. Biomech.* **40**, 1794–1805 (2007)
25. Müller, L.O., Toro, E.F.: A global multiscale mathematical model for the human circulation with emphasis on the venous system. *Int. J. Numer. Methods Biomed. Eng.* **30**, 681–725 (2014)
26. Liang, F.Y., Takagi, S., Himeno, R., et al.: A computational model of the cardiovascular system coupled with an upper-arm oscillometric cuff and its application to studying the suprasystolic cuff oscillation wave concerning its value in assessing arterial stiffness. *Comput. Methods Biomech. Biomed. Eng.* **16**, 141–157 (2013)
27. Pan, Q., Wang, R., Reglin, B., et al.: A one-dimensional mathematical model for studying the pulsatile flow in microvascular networks. *J. Biomech. Eng.* **136**, 011009 (2014)
28. Frank, O.: Die grundform des arteriellen pulses. *Z. Biol.* **37**, 483–526 (1899)
29. Westerhof, N., Lankhaar, J.W., Westerhof, B.E.: The arterial windkessel. *Med. Biol. Eng. Comput.* **47**, 131–141 (2009)
30. Westerhof, N., Bosman, F., De Vries, C.J., et al.: Analog studies of the human systemic arterial tree. *J. Biomech.* **2**, 121–143 (1969)
31. Stergiopoulos, N., Westerhof, B.E., Westerhof, N.: Total arterial inertance as the fourth element of the windkessel model. *Am. J. Physiol.* **276**, H81–H88 (1999)
32. Liang, F.Y., Liu, H.: Simulation of hemodynamic responses to the valsalva maneuver: an integrative computational model of the cardiovascular system and the autonomic nervous system. *J. Physiol. Sci.* **56**, 45–65 (2006)
33. Lu, K., Clark, J.W.J., Ghorbel, F.H., et al.: A human cardiopulmonary system model applied to the analysis of the valsalva maneuver. *Am. J. Physiol. Heart Circ. Physiol.* **281**, H2661–H2679 (2001)
34. Stergiopoulos, N., Young, D.F., Rogge, T.: Computer simulation of arterial flow with applications to arterial and aortic stenosis. *J. Biomech.* **25**, 1477–1488 (1992)
35. Olufsen, M.S., Peskin, C.S., Kim, W.Y., et al.: Numerical simulation and experimental validation of blood flow in arteries with structured-tree outflow conditions. *Ann. Biomed. Eng.* **28**, 1281–1299 (2000)
36. Heywood, J.G., Rannacher, R., Turek, S.: Artificial boundaries and flux and pressure conditions for the incompressible Navier–Stokes equations. *Int. J. Numer. Methods Fluids.* **22**, 325–352 (1996)
37. Formaggia, L., Moura, A., Nobile, F.: On the stability of the coupling of 3D and 1D fluid–structure interaction models for blood flow simulations. *ESAIM Math. Model. Numer. Anal.* **41**, 743–769 (2007)
38. Leiva, J.S., Blanco, P.J., Buscaglia, G.C.: Iterative strong coupling of dimensionally heterogeneous models. *Int. J. Numer. Methods Eng.* **81**, 1558–1580 (2009)
39. Leiva, J.S., Blanco, P.J., Buscaglia, G.C.: Partitioned analysis for dimensionally-heterogeneous hydraulic networks. *Multiscale Model. Simul.* **9**, 872–903 (2011)
40. Vignon-Clementel, I.E., Figueroa, C.A., Jansen, K.E., et al.: Outflow boundary conditions for three-dimensional finite element modeling of blood flow and pressure in arteries. *Comput. Methods Appl. Mech. Eng.* **195**, 3776–3796 (2006)
41. Blanco, P.J., Pivello, M.R., Urquiza, S.A., et al.: On the potentialities of 3D–1D coupled models in hemodynamics simulations. *J. Biomech.* **42**, 919–930 (2009)

42. Hsia, T.Y., Cosentino, D., Corsini, C., et al.: Use of mathematical modeling to compare and predict hemodynamic effects between hybrid and surgical Norwood palliations for hypoplastic left heart syndrome. *Circulation* **124**, S204–S210 (2011)
43. Mahler, F., Muheim, M.H., Intaglietta, M., et al.: Blood pressure fluctuations in human nailfold capillaries. *Am. J. Physiol. Heart Circ. Physiol.* **236**, H888–H893 (1979)
44. Nakano, T., Tominaga, R., Nagano, I., et al.: Pulsatile flow enhances endothelium-derived nitric oxide release in the peripheral vasculature. *Am. J. Physiol. Heart Circ. Physiol.* **278**, H1098–H1104 (2000)
45. Li, Y., Zheng, J., Bird, I.M., et al.: Effects of pulsatile shear stress on nitric oxide production and endothelial cell nitric oxide synthase expression by ovine fetoplacental artery endothelial cells. *Biol. Reprod.* **69**, 1053–1059 (2003)
46. Uryash, A., Wu, H., Bassuk, J., et al.: Low-amplitude pulses to the circulation through periodic acceleration induces endothelial-dependent vasodilatation. *J. Appl. Physiol.* **106**, 1840–1847 (2009)
47. Sezai, A., Shiono, M., Orime, Y., et al.: Renal circulation and cellular metabolism during left ventricular assisted circulation: comparison study of pulsatile and nonpulsatile assists. *Artif. Organs.* **21**, 830–835 (1997)
48. Orime, Y., Shiono, M., Nakata, et al.: The role of pulsatility in end-organ microcirculation after cardiogenic shock. *ASAIO J.* **42**, M724–728 (1996)
49. O’Neil, M.P., Fleming, J.C., Badhwar, A., et al.: Pulsatile versus nonpulsatile flow during cardiopulmonary bypass: microcirculatory and systemic effects. *Ann. Thorac. Surg.* **94**, 2046–2053 (2012)
50. Mittal, N., Zhou, Y., Linares, C., et al.: Analysis of blood flow in the entire coronary arterial tree. *Am. J. Physiol. Heart Circ. Physiol.* **289**, H439–H446 (2005)
51. Lipowsky, H.H., Zweifach, B.W.: Network analysis of microcirculation of cat mesentery. *Microvasc. Res.* **7**, 73–83 (1974)
52. Pries, A.R., Secomb, T.W., Gaehtgens, P., et al.: Blood flow in microvascular networks. Experiments and simulation. *Circ. Res.* **67**, 826–834 (1990)
53. Grinberg, L., Cheever, E., Anor, T., et al.: Modeling blood flow circulation in intracranial arterial networks: a comparative 3D/1D simulation study. *Ann. Biomed. Eng.* **39**, 297–309 (2011)
54. Shi, Y., Lawford, P., Hose, R.: Review of zero-D and 1-D models of blood flow in the cardiovascular system. *Biomed. Eng. Online* **10**, 33 (2011)
55. Ganesan, P., He, S., Xu, H.: Modelling of pulsatile blood flow in arterial trees of retinal vasculature. *Med. Eng. Phys.* **33**, 810–823 (2011)
56. Lee, J., Smith, N.: Development and application of a one-dimensional blood flow model for microvascular networks. *Proc. Inst. Mech. Eng. Part H* **222**, 487–511 (2008)
57. Seki, J.: Flow pulsation and network structure in mesenteric microvasculature of rats. *Am. J. Physiol. Heart Circ. Physiol.* **266**, H811–H821 (1994)
58. Pries, A.R., Ley, K., Gaehtgens, P.: Generalization of the Fahraeus principle for microvessel networks. *Am. J. Physiol. Heart Circ. Physiol.* **251**, H1324–1332 (1986)
59. Nakano, A., Sugii, Y., Minamiyama, M., et al.: Measurement of red cell velocity in microvessels using particle image velocimetry (PIV). *Clin. Hemorheol. Microcirc.* **29**, 445–455 (2003)
60. Golub, A.S., Barker, M.C., Pittman, R.N.: Microvascular oxygen tension in the rat mesentery. *Am. J. Physiol. Heart Circ. Physiol.* **294**, H21–H28 (2008)
61. Pries, A.R., Secomb, T.W.: Origins of heterogeneity in tissue perfusion and metabolism. *Cardiovasc. Res.* **81**, 328–335 (2009)
62. Tuma, R.F., Duran, W.N., Ley, K.: *Microcirculation*. Academic Press, New York (2008)
63. Fung, Y.C., Zweifach, B.W., Intaglietta, M.: Elastic environment of the capillary bed. *Circ. Res.* **19**, 441–461 (1966)
64. Pries, A.R., Secomb, T.W., Gaehtgens, P.: Biophysical aspects of blood flow in the microvasculature. *Cardiovasc. Res.* **32**, 654–667 (1996)
65. Alastruey, J., Parker, K.H., Peiro, J., et al.: Lumped parameter outflow models for 1-D blood flow simulations: effect on pulse waves and parameter estimation. *Commun. Comput. Phys.* **4**, 317–336 (2008)
66. Dao, M., Lim, C.T., Suresh, S.: Mechanics of the human red blood cell deformed by optical tweezers. *J. Mech. Phys. Solids* **51**, 2259–2280 (2003)
67. Tsubota, K., Wada, S.: Elastic force of red blood cell membrane during tank-treading motion: consideration of the membrane’s natural state. *Int. J. Mech. Sci.* **52**, 356–364 (2010)
68. Tsubota, K., Wada, S.: Effect of the natural state of an elastic cellular membrane on tank-treading and tumbling motions of a single red blood cell. *Phys. Rev. E.* **81**, 011910 (2010)
69. Tsubota, K., Wada, S., Liu, H.: Elastic behavior of a red blood cell with the membrane’s nonuniform natural state: equilibrium shape, motion transition under shear flow, and elongation during tank-treading motion. *Biomech. Model. Mechanobiol.* **13**, 735–746 (2014)
70. Skalak, R., Tozeren, A., Zarda, R.P., et al.: Strain energy function of red blood cell membranes. *Biophys. J.* **13**, 245–264 (1973)
71. Helfrich, W.: Elastic properties of lipid bilayers: theory and possible experiments. *Z. Naturforsch. C.* **28**, 693–703 (1973)
72. Tsubota, K.: Short note on the bending models for a membrane in capsule mechanics: comparison between continuum and discrete models. *J. Comput. Phys.* **277**, 320–328 (2014)
73. Kamada, H., Tsubota, K., Nakamura, M., et al.: A three-dimensional particle simulation of the formation and collapse of a primary thrombus. *Int. J. Numer. Methods Biomed. Eng.* **26**, 488–500 (2010)
74. Kamada, H., Tsubota, K., Nakamura, M., et al.: Computational study on effect of stenosis on primary thrombus formation. *Biorheology* **48**, 99–114 (2011)
75. Miyoshi, H., Tsubota, K., Hoyano, T., et al.: Three-dimensional modulation of cortical plasticity during pseudopodial protrusion of mouse leukocytes. *Biochem. Biophys. Res. Commun.* **438**, 594–599 (2013)
76. Tsubota, K., Wada, S., Yamaguchi, T.: Simulation study on effects of hematocrit on blood flow properties using particle method. *J. Biomech. Sci. Eng.* **1**, 159–170 (2006)
77. Morishita, Y., Iwasa, Y.: Growth based morphogenesis of vertebrate limb bud. *Bull. Math. Biol.* **70**, 1957–1978 (2008)
78. Morishita, Y., Suzuki, T.: Bayesian inference of whole-organ deformation dynamics from limited space-time point data. *J. Theor. Biol.* **357**, 74–85 (2014)
79. Ishihara, S., Sugimura, K.: Bayesian inference of force dynamics during morphogenesis. *J. Theor. Biol.* **313**, 201–211 (2012)
80. Okuda, S., Inoue, Y., Eiraku, M., et al.: Reversible network reconnection model for simulating large deformation in dynamic tissue morphogenesis. *Biomech. Model. Mechanobiol.* **12**, 627–644 (2013)
81. Ridley, A.J., Schwartz, M.A., Burridge, K., et al.: Cell migration: integrating signals from front to back. *Science* **302**, 1704–1709 (2003)
82. Mullins, R.D., Heuser, J.A., Pollard, T.D.: The interaction of Arp2/3 complex with actin: nucleation, high affinity pointed end capping, and formation of branching networks of filaments. *Proc. Natl. Acad. Sci. USA* **95**, 6181–6186 (1998)

83. Svitkina, T.M., Borisy, G.G.: Arp2/3 complex and actin depolymerizing factor/cofilin in dendritic organization and treadmilling of actin filament array in lamellipodia. *J. Cell Biol.* **145**, 1009–1026 (1999)
84. Pollard, T.D., Blanchoin, L., Mullins, D.: Molecular mechanisms controlling actin filament dynamics in nonmuscle cells. *Annu. Rev. Biophys. Biomol. Struct.* **29**, 545–576 (2000)
85. Small, J.V., Stradal, T., Vignall, E., et al.: The lamellipodium: where motility begins. *Trends Cell Biol.* **12**, 112–120 (2002)
86. Chhabra, E.S., Higgs, H.N.: The many faces of actin: matching assembly factors with cellular structures. *Nat. Cell Biol.* **9**, 1110–1121 (2007)
87. Lazarides, E., Burridge, K.: α -Actinin: immunofluorescent localization of a muscle structural protein in nonmuscle cells. *Cell* **6**, 289–298 (1975)
88. Weber, K., Groeschel-Stewart, U.: Antibody to myosin: the specific bisualization of myosin-containing filaments in nonmuscle cells. *Proc. Natl. Acad. Sci. USA* **71**, 4561–4564 (1974)
89. Small, J.V., Rottner, K., Kaverina, I., et al.: Assembling an actin cytoskeleton for cell attachment and movement. *Biochim. Biophys. Acta* **1404**, 271–281 (1998)
90. Hotulainen, P., Lappalainen, P.: Stress fibers are generated by two distinct actin assembly mechanisms in motile cells. *J. Cell Biol.* **173**, 383–394 (2006)
91. Pellegrin, S., Mellor, H.: Actin stress fibres. *J. Cell Sci.* **120**, 3491–3499 (2007)
92. Chiu, J.J., Chien, S.: Effects of disturbed flow on vascular endothelium: pathophysiological basis and clinical perspectives. *Physiol. Rev.* **91**, 327–387 (2011)
93. Ward, M.R., Pasterkamp, G., Yeung, A.C., et al.: Arterial remodeling: mechanisms and clinical implications. *Circulation* **102**, 1186–1191 (2000)
94. Wojciak-Stothard, B., Ridley, A.J.: Shear stress-induced endothelial cell polarization is mediated by Rho and Rac but not Cdc42 or PI 3-kinases. *J. Cell Biol.* **161**, 429–439 (2003)
95. Ingber, D.E.: Tensegrity II: how structure networks influence cellular information processing networks. *J. Cell Sci.* **116**, 1397–1408 (2003)
96. Schwartz, E.A., Gerristen, M.E., Bizios, R.: Effects of Hydrostatic Pressure on Endothelial Cells. In: Lelkes, P. I. (ed.) *Endothelium and Mechanical Forces*, chapter 13, pp. 275–290. Harwood Academic Publishers, London, England (1999)
97. Chien, S.: Effects of disturbed flow on endothelial cells. *Ann. Biomed. Eng.* **36**, 554–562 (2008)
98. Azuma, N., Aydin Duzgan, S., Ikeda, M., et al.: Endothelial cell response to different mechanical forces. *J. Vasc. Surg.* **32**, 789–794 (2000)
99. Davies, P.F., Tripathi, S.C.: Mechanical stress mechanisms and the cell. An endothelial paradigm. *Circ. Res.* **72**, 239–245 (1993)
100. Chicurel, M.E., Chen, C.S., Ingber, D.E.: Cellular control lies in the balance of forces. *Curr. Opin. Cell Biol.* **10**, 232–239 (1998)
101. Seneviratne, A., Hulsmans, M., Holvoet, P., et al.: Biomechanical factors and macrophages in plaque stability. *Cardiovasc. Res.* **99**, 284–293 (2013)
102. Gao, H., Long, Q.: *Atherosclerosis Plaque Stress Analysis: A Review*, vol. XIX. Springer, New York (2014)
103. Yim, P., DeMarco, K., Castro, M.A., et al.: Characterization of shear stress on the wall of the carotid artery using magnetic resonance imaging and computational fluid dynamics. *Stud. Health Technol. Inform.* **113**, 412–442 (2005)
104. Barbee, K.A., Davies, P.F., Lal, R.: Shear stress-induced reorganization of the surface topography of living endothelial cells imaged by atomic force microscopy. *Circ. Res.* **74**, 163–171 (1994)
105. Wei, T., Nackman, G.B., Voorhees, A.: Experiments show importance of flow-induced pressure on endothelial cell shape and alignment. *Proc. R. Soc. A* **463**, 1409–1419 (2007)
106. Liu, S.Q., Yen, M., Fung, Y.C.: On measuring the third dimension of cultured endothelial cells in shear flow. *Proc. Natl. Acad. Sci. USA* **91**, 8782–9796 (1994)
107. Hazel, A.L., Pedley, T.J.: Vascular endothelial cells minimize the total force on their nuclei. *Biophys. J.* **78**, 47–54 (2000)
108. Waché, P., Wang, X., Maurice, et al.: Calcul numérique de la déformation mécanique d'un modèle de cellule endothéliale. *C. R. Acad. Sci. Paris Biomécan./Biomech.* **328**, 633–638 (2000) (in German)